scientific reports

Check for updates

OPEN

Energy transfer in Carreau Yasuda liquid influenced by engine oil with Magnetic dipole using tri-hybrid nanoparticles

Muhammad Bilal[1], Ikram Ullah[2], Mohammad Mahtab Alam[3], Syed Irfan Shah[4] & Sayed M. Eldin[5]✉

The aim of the current analysis is to evaluate the significances of magnetic dipole and heat transmission through ternary hybrid Carreau Yasuda nanoliquid flow across a vertical stretching sheet. The ternary compositions of Al_2O_3, SiO_2, and TiO_2 nanoparticles (nps) in the Carreau Yasuda fluid are used to prepare the ternary hybrid nanofluid (Thnf). The heat transfer and velocity are observed in context of heat source/sink and Darcy Forchhemier effect. Mathematically, the flow scenario has been expressed in form of the nonlinear system of PDEs for fluid velocity and energy propagation. The obtained set of PDEs are transform into ODEs through suitable replacements. The obtained dimensionless equations are computationally solved with the help of the parametric continuation method. It has been observed that the accumulation of Al_2O_3, SiO_2 and TiO_2-nps to the engine oil, improves the energy and momentum profiles. Furthermore, as compared to nanofluid and hybrid nanofluid, ternary hybrid nanofluid have a greater tendency to boost the thermal energy transfer. The fluid velocity lowers with the outcome of the ferrohydrodynamic interaction term, while enhances with the inclusion of nano particulates (Al_2O_3, SiO_2 and TiO_2).

List of symbols

v, u	Velocity components
μ_0	Magnetic permeability
C_p	Specific heat
T	Temperature
π	*Pi*
σ	Electrical conductivity
nps	Nanoparticles
p	Pressure
k	Thermal conductivity
T_w	Wall temperature
Nu	Nusselt number
M	Magnetization
H_t	Heat source
$\theta(\eta)$	Energy field
β	Ferrohydrodynamic term
We	Weissenberg number
Al_2O_3	Aluminum oxide
Ec	Eckert number
ρ	Density
Λ	Carreau Yasuda number

[1]Sheikh Taimur Academic Block-II, Department of Mathematics, University of Peshawar, Peshawar 25120, Khyber Pakhtunkhwa, Pakistan. [2]Department of Natural Sciences and Humanities, University of Engineering and Technology, Mardan 23200, Pakistan. [3]Department of Basic Medical Sciences, College of Applied Medical Science, King Khalid University, Abha 61421, Saudi Arabia. [4]Department of Sciences and Humanities, National University of Computer and Emerging Sciences, Islamabad 44000, Pakistan. [5]Center of Research, Faculty of Engineering, Future University in Egypt, New Cairo 11835, Egypt. ✉email: sayed.eldin22@fue.edu.eg

Q_0	Heat source
u_e	Free stream velocity
λ	Viscous dissipation
Re	Reynolds number
Thnf	Trihybrid nanofluid
γ	Strength of the magnetic dipole
S_1	Stretching ratio number
ε	Ratio parameter
C_f	Skin fraction
Pr	Prandtl number
φ	Nanoparticles volume friction
$f'(\eta)$	Velocity profile
Fr	Darcy Forchhemier term
m	Power-law number
SiO_2	Silicon dioxide
TiO_2	Titanium dioxide

The study of simple or hybrid nanofluid flow across a vertical surface, wither stretching or rigid plate with energy allocation characteristics has major commitment in recent developments and industrial uses[1]. Recently, Shah et al.[2] documented the upshot of molecular diffusion on the flow characteristics of nanoliquid with concentration diffusivity and variable viscosity across a vertical sheet. It was revealed that greater temperature-dependent viscous factors improve velocity curve in both assisting and opposing flows. Chen et al.[3] used computation algorithm to evaluate the fluid flows across a vertical surface, at Fr = 1.1 and Re = 2.7 105. Singh and Seth[4] investigated the mass and thermal mobility behavior of MHD fluid flow inside a vertical stream bounded by the highly permeable regime using the Hall characteristic and an induced magnetic field. Shafiq et al.[5] established a mathematical bioconvective model to analyze the thermodynamically thixotropic nanomaterials flow by implementing thermal radiation and convective conditions. The conclusions indicated that they can be utilised to improve heating and cooling procedures, manufacturing and energy generation among other factors. Fayz-Al-Asad et al.[6] evaluated the MHD Maxwell fluid flow in conjunction with thermal conductivity and heat dependent viscosity along a stratified vertical surface using nth order fusion reaction. Sharma and Gandhi[7] reviewed an unsteady MHD fluid flow across a vertical elongating surface implanted in a Darcy-Forchheimer permeable material with first-order chemical reaction and heat source/sink. Sharma et al.[8] investigated an incompressible fluid flow across a variable vertical elongating sheet with additional effects of Ohmic heating, viscous dissipation, thermophoresis, thermal heat source, Brownian motion, activation energy and exponential heat source. The solar thermal transport features of hybrid nanoliquid in the existence of an external electromagnetic effect, radiation and heat source are investigated Rizk et al.[9]. Rooman et al.[10] considered the enhancement of transfer of thermal energy in tri-hybrid Ellis nanoliquid flow when a magnetic polarization moves across a vertical substrate. It was discovered that the energy pattern advances with modification in heat generation and viscous dissipation. A magnetic dipole makes a substantial impact to the power generation, and an inverse correlation is indicated versus the flow pattern. Some recent analysis may be found in Ref.[11–14].

Nanotechnology is an exciting scientific discipline with numerous implementations that range from skincare brands, groceries, apparels, and home electronics to fuel catalysts, therapeutic approaches, and alternative resources. Construction activities, nanomachining of nanostructures, nanowires, nanosheets, water purifiers, and waste management are all examples of how nanotechnology is being used in advanced manufacturing and detoxification operations[15–17]. Their implementations are expanding to include "nanomedicine" by fusing nanostructures with microbial macromolecules or frameworks, "green technology" to improve sustainable development, and "renewable energy" to establish new methods of capturing, storing, and transferring energy. Nanofiber generation, for example, has been used in applications like energy storage batteries, auto parts, thin-film telecommunications equipment, varnishes, and many more[18–20]. But such applications and uses of nanofluid in advanced techniques is only possible due to the involvement of hybrid and ternary nanofluid. Therefore, in the current analysis, we have used Al_2O_3, SiO_2, and TiO_2 in the engine oil. Okumura et al.[21] used the Al_2O_3, TiO_2 and SiO_2, for the oxidation of H_2 and CO for chemical vapor deposition of gold. Minea[22] calculated the properties of oxide-based hybrid nanofluid (Al_2O_3, TiO_2 and SiO_2) and their derivatives. All type of nanoliquid' thermal performance changed with the inclusion of nanoparticles, and thermal expansion increased by at least 12%. Said et al.[23] presented an experimental analysis on the density and stability of Al_2O_3, TiO_2, $TiSiO_4$ and SiO_2. Minea[24] Khan worked on a complex mathematical model on the energy transport efficiency and hydrostatic power of nanoliquids for a fluid dynamic assessment. The best flow behavior was observed when water was replaced with SiO_2–Al_2O_3hybrid nanofluids. Abbasi et al.[25] disclosed a correlative thermal evaluation of three sorts of nanoparticles, including aluminum oxide (Al_2O_3), titanium dioxide (TiO_2) and silicon dioxide (SiO_2) with the ethylene glycol base fluid over a circular cylinder containing the point of stagnation. Dadheech et al.[26] reviewed the flow of an SiO2-Al2O3-TiO2/C2H6O2-based modified ferrofluid along an extending substrate. It was discovered that the thermal transfer capacity of modified nanoliquids is greater than that of simple and hybrid nanoliquids. Erkan et al.[27] used Al_2O_3, TiO_2, and SiO_2 in ethylene glycol for engine radiator applications. As a result, using TiO_2 particles yielded the highest energy conversion efficiency (35.67%). Alharbi et al.[28–30] created a nanofluid model with TiO_2 in the base fluid within a squeezing/dilating channel, which included nanoparticle accumulation effects and nonlinear thermal radiations. The outcome confirmed that the fluid mobility is substantially controlled by the high viscosity variation caused by nanomaterials aggregation. Furthermore, thermal radiations

generate significant heat, which can be used to break down the accumulation of the nanomaterials. Some recent studies may be found in Ref.[31–34].

A magnetic dipole is made up of two magnetic poles isolated by a small distance. A magnetic moment is a unit of measurement that signifies the magnetic strength and alignment of a magnet or other component that generates a magnetic field. The consequences of magnetic dipole on trihybrid nanoliquid flow are evaluated. Magnetic dipole fused with trihybrid nanoliquid performs an important function in energy transference[35]. The effectiveness of 2D Oldroyd-B fluid flow across a shrinking sheet with thermal buoyancy was highlighted by Bashir et al.[36]. The findings demonstrated that as the thermal relaxation time factor's value boosts, the proportion of heat transport lowers. Additionally, the rate of thermophoretic accumulation slows down as the thermophoretic index rises. To analyse the innovative fluid flow in the existence of magnetic dipoles, Shoaib et al.[37] described the artificial neural network with Levenberg–Marquardt algorithm that is intelligence-based.

The objective of the current assessment is to evaluate the significances of magnetic dipole and heat transmission through ternary hybrid Carreau Yasuda nanoliquid flow across a vertical stretching sheet. The ternary compositions of Al_2O_3, SiO_2, and TiO_2-nps in the Carreau Yasuda fluid are used to prepare the ternary hybrid nanofluid (Thnf). The heat transfer and velocity are observed in context of heat source/sink and Darcy Forchhemier effect. Mathematically, the flow scenario has been expressed in form of the nonlinear system of PDEs for fluid velocity and energy propagation. The acquired set of PDEs are transform into ODEs through suitable substitutions. The obtained dimensionless equations are computationally solved with the help of the PCM. In the coming segment, the flow set-up has been verbalized, solved and discussed.

Mathematical analysis

The 2D Carreau Yasuda fluid with energy transfer is considered across an extending vertical sheet using ternary nanocomposites (TiO_2, Al_2O_3 and SiO_2). The Carreau Yasuda liquid is engrossed with base fluid (engine oil) in the Darcy medium. Three distinct kinds of nanocomposites (TiO_2, Al_2O_3 and SiO_2) are scattered in the base fluid. Surface of the wall is supposed to be stretchy to cause fluid motion. Hence, the fluid flow is due to the stretching of the sheet. Horizontally, the magnetic dipole is assumed to be in center as demonstrated in Fig. 1. The x & y-axis are taken in horizontal and vertical side of the sheet. The energy propagation is counted under the consequences of heat source. Based on the above suppositions, the modeled equations are formulated as[38,39]:

$$\frac{\partial u}{\partial x}+\frac{\partial v}{\partial y}=0, \tag{1}$$

$$\rho_{Thnf}\left(u\frac{\partial u}{\partial x}+v\frac{\partial u}{\partial y}\right)=-\frac{\partial P}{\partial x}+\mu_0 M\frac{\partial H}{\partial x}+\nu_{hnf}\left(\frac{\partial^2 u}{\partial y^2}+\Lambda^d\left(\frac{m-1}{d}\right)(d+1)\frac{\partial^2 u}{\partial y^2}\left(\frac{\partial u}{\partial y}\right)^d\right)-\frac{\mu_{nf}}{\rho_{nf}K}u-\frac{c_b}{\sqrt{K}}u^2, \tag{2}$$

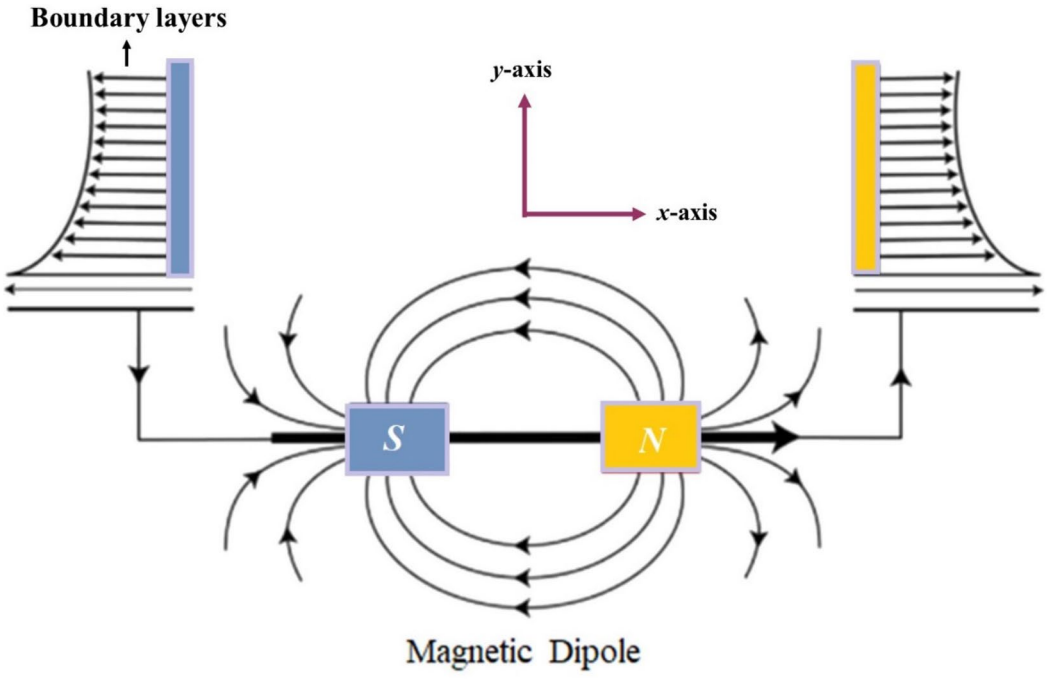

Figure 1. Fluid flow geometrical illustration.

$$(\rho C_p)_{Thnf}\left(u\frac{\partial T}{\partial x}+v\frac{\partial T}{\partial y}\right)+\mu_0\left(u\frac{\partial H}{\partial x}+v\frac{\partial H}{\partial y}\right)T\frac{\partial M}{\partial T}=K_{Thnf}\frac{\partial^2 T}{\partial y^2}+Q_0(T-T_\infty). \tag{3}$$

The boundary conditions are:

$$u=sx,\ \ v=0,\ \ T=T_w,\ \ u=0,\ \ T=T_\infty. \tag{4}$$

The scalar potential with magnetic force is specified as:

$$\beta=\frac{\delta}{2\pi}\left(\frac{x}{x^2+(y+d)^2}\right). \tag{5}$$

x-axis and y-axis terms magnetic inductions are:

$$H_x=\frac{-\partial\delta}{\partial x}=\frac{\delta}{2\pi}\left(\frac{x-(d+y)^2}{\left(x^2+(d+y)^2\right)^2}\right), \tag{6}$$

$$H_y=\frac{-\partial\delta}{\partial y}=\frac{\delta}{2\pi}\left(\frac{2x(d+y)}{\left(x^2+(d+y)^2\right)^2}\right). \tag{7}$$

The magnitude of magnetic induction is

$$H=\left[\left(\frac{\partial\delta}{\partial y}\right)^2+\left(\frac{\partial\delta}{\partial x}\right)^2\right]^{12}. \tag{8}$$

$$H_b=\frac{\partial\delta}{\partial b}\left(\frac{-2}{(d+b)^3}+\frac{4a^2}{(d+b)^5}\right),\ \ H_a=\frac{\partial\delta}{\partial b}\left(\frac{-2a}{(d+b)^4}\right). \tag{9}$$

The resemblance substitution is:

$$u=sxf',\ \ v=-(sv_f)^{\frac{1}{2}}f,\ \ \theta=\frac{T_\infty-T}{T_\infty-T_w},\ \ \eta=y\sqrt{\frac{s}{y}} \tag{10}$$

The obtained dimensionless system of ODEs is:

$$f'''+(We)^d\frac{(m-1)(d+1)}{d}f''''(f'')^d-\frac{\nu_{Thnf}}{\nu_f}\left(f'^2-ff''+\frac{2\beta\theta\rho_f}{(\eta+\gamma)^4}\right)-Fr(f')^2-krf'. \tag{11}$$

$$\begin{aligned}&\theta''+\frac{(\rho C_p)_{Thnf}k_f}{(\rho C_p)_f k_{Thnf}}Pr(f\theta'-2f'\theta)+\frac{(\rho C_p)_{Thnf}k_f}{(\rho C_p)_f k_{Thnf}}\frac{2\beta\lambda f(\theta-\varepsilon)}{(\eta+\gamma)^3}+\frac{k_f(PrH_t\theta)}{k_{Thnf}}-\frac{k_f}{k_{Thnf}}\\&\frac{4\lambda(1-\phi_2)^{-2.5}}{(1-\phi_1)^{2.5}(1-\phi_3)^{2.5}}(f'')^2=0,\end{aligned} \tag{12}$$

The transform boundary conditions are:

$$\begin{aligned}&f(0)=0,\quad \theta(0)=1,\ \ f'(0)=1,\\&f'(\infty)=0,\ \theta(\infty)=0.\end{aligned} \tag{13}$$

The non- dimensional parameters are: $\beta=\frac{\gamma}{2\pi}\frac{\mu_0(T_\infty-T_w)\rho}{\mu^2}, Pr=\frac{\nu}{\alpha}, \varepsilon=\frac{T_\infty}{T_\infty-T_w}, \lambda=\frac{su}{\rho K(T_\infty-T_w)}$, $\gamma=\sqrt{\frac{s\rho c^2}{\mu}}, H_t=\frac{Q_0}{b(\rho C_p)_{bf}}$. It is observed that Eq. (11), (12) are non-Newtonian fluid model. The non-Newtonian model may be simplified to Newtonian case by putting $\beta=0$ and $We=0$.

The skin friction is expressed as:

$$\sqrt{Re}C_f=\frac{-\left(\frac{m-1}{d}We^2(f''(0))^d+1\right)f''(0)}{(1-\phi_3)^{2.5}(1-\phi_2)^{2.5}(1-\phi_1)^{2.5}}, \tag{14}$$

The Nusselt number is expressed as:

$$(Re)^{\frac{-1}{2}}Nu=\frac{-K_f}{K_{Thnf}}\theta'(0) \tag{15}$$

Numerical solution

The core steps, while solving Eqs. (11)–(13) through parametric continuation method are as follow[41–43]:

Step 1: reducing the system of BVP to 1st order.

$$q_1 = f(\eta),\ \ q_2 = f'(\eta),\ \ q_3 = f''(\eta),\ \ q_4 = \theta(\eta),\ \ q_5 = \theta'(\eta). \tag{16}$$

By using Eq. (16) in Eqs. (11)–(13), we get:

$$q_3' + (We)^d \frac{(m-1)(d+1)}{d} q_3' (q_3)^d - \frac{\nu_{Thnf}}{\nu_f}\left(q_2^2 - q_1 q_3 + \frac{2\beta q_4 \rho_f}{(\eta+\gamma)^4}\right) - Fr(q_2)^2 - kr\, q_2. \tag{17}$$

$$\begin{aligned} &q_5' + \frac{(\rho C_p)_{Thnf} k_f}{(\rho C_p)_f k_{Thnf}} Pr(q_1 q_5 - 2 q_2 q_4) + \frac{(\rho C_p)_{Thnf} k_f}{(\rho C_p)_f k_{Thnf}} \frac{2\beta\lambda q_1 (q_4 - \varepsilon)}{(\eta+\gamma)^3} + \frac{k_f (PrH_t q_4)}{k_{Thnf}} \\ &- \frac{k_f}{k_{Thnf}} \frac{4\lambda(1-\phi_2)^{-2.5}}{(1-\phi_1)^{2.5}(1-\phi_3)^{2.5}} (q_3)^2 = 0, \end{aligned} \tag{18}$$

with the corresponding boundary conditions

$$\begin{aligned} &q_1(0) = 0,\ \ q_2(0) = 1,\ \ q_4(0) = 1, \\ &q_2(\infty) = 0,\ \ q_4(\infty) = 0. \end{aligned} \tag{19}$$

Step 2: presenting the embedding constraint p in Eqs. (17)–(19).

$$q_3' + (We)^d \frac{(m-1)(d+1)}{d} q_3' (q_3 - 1)^d p - \frac{\nu_{Thnf}}{\nu_f}\left(q_2^2 - q_1 q_3 + \frac{2\beta q_4 \rho_f}{(\eta+\gamma)^4}\right) - Fr(q_2)^2 - kr\, q_2. \tag{20}$$

$$\begin{aligned} &q_5' + \frac{(\rho C_p)_{Thnf} k_f}{(\rho C_p)_f k_{Thnf}} Pr(q_1 (q_5 - 1) p - 2 q_2 q_4) + \frac{(\rho C_p)_{Thnf} k_f}{(\rho C_p)_f k_{Thnf}} \frac{2\beta\lambda q_1 (q_4 - \varepsilon)}{(\eta+\gamma)^3} + \frac{k_f (PrH_t q_4)}{k_{Thnf}} \\ &- \frac{k_f}{k_{Thnf}} \frac{4\lambda(1-\phi_2)^{-2.5}}{(1-\phi_1)^{2.5}(1-\phi_3)^{2.5}} (q_3)^2 = 0, \end{aligned} \tag{21}$$

Results and discussion

The trend physical process and behind each Table and figure are elaborated in this section. This section also revealed the velocity $f'(\eta)$ and energy $\theta(\eta)$ profiles outlines versus physical constraints.

Figures 2, 3, 4, 5, 6, 7 display the velocity profile $f'(\eta)$ outlines versus ferrohydrodynamic interaction number β, ternary nanoparticles $\varphi(\eta)$, Weissenberg number We, power-law number m, Darcy Forchhemier term Fr and porosity term kr respectively. The variance in velocity profile versus the significance β is depicted in Fig. 2. It has been observed that a magnetic dipole draws fluid molecules at the wall's surface and that this pulling of fluid droplets toward the magnetic dipole causes friction between layers and particles. Hence, the velocity of fluid particles slows down. As a result, the fact that velocity curves have a decreasing function against the consequences β, is incorporated. The graph is examined in both the absence of a dipole and the presence of a magnetic dipole.

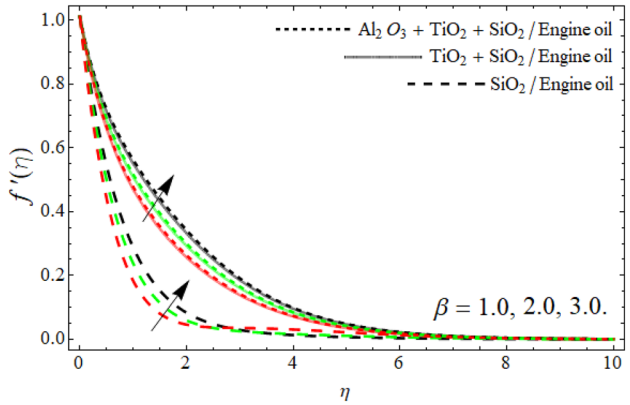

Figure 2. Velocity $f'(\eta)$ field versus ferrohydrodynamic interaction number β.

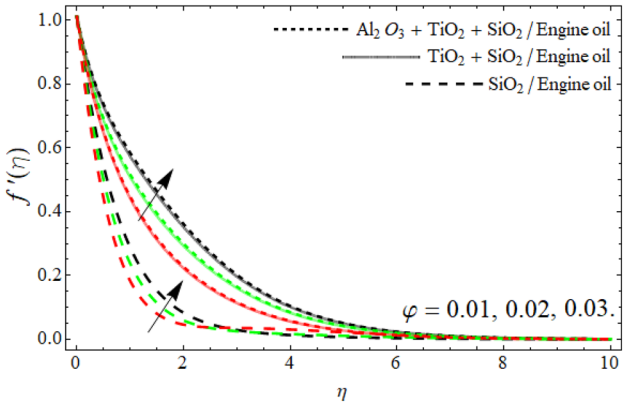

Figure 3. Velocity $f'(\eta)$ field versus ternary nanoparticles φ.

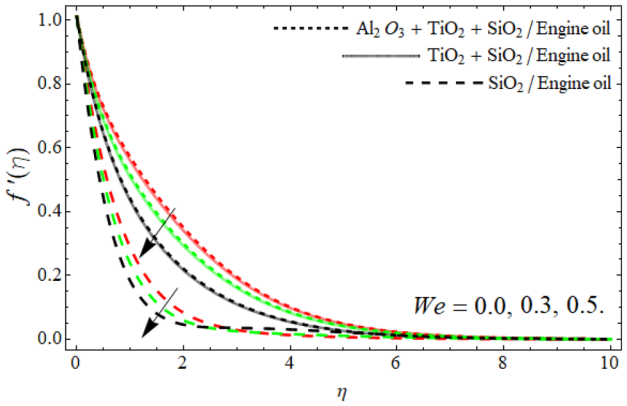

Figure 4. Velocity $f'(\eta)$ field versus Weissenberg number We.

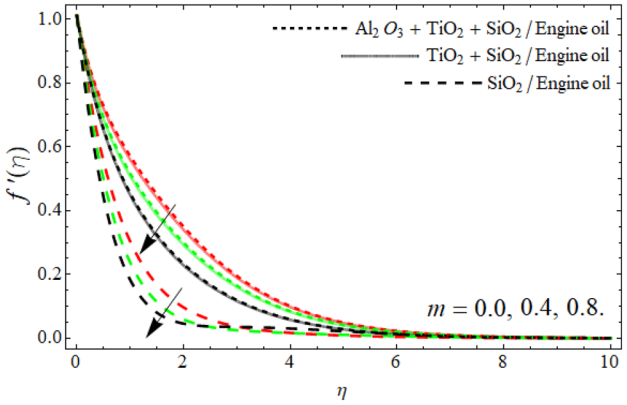

Figure 5. Velocity $f'(\eta)$ field versus power law number m.

Figure 3 reported that the inclusion of nano particulates in the base fluid augments the momentum profile. The density of engine oil as compared to Al_2O_3, SiO_2 and TiO_2 is much higher. Therefore, the insertion of these nanoparticles into the engine oil reduces its average density, as a result, the velocity contour enhances. Figures 4 and 5 show that the velocity $f'(\eta)$ declines with the upshot of We and power-law number m. A Weissenberg number is a physical ratio between elastic and viscous forces. It can be shown that an increase in We leads to an upsurge in the viscosity of fluid particles. As a result, the fluid becomes much thicker and reduces the number of layers of momentum boundary as elaborated in Fig. 4.

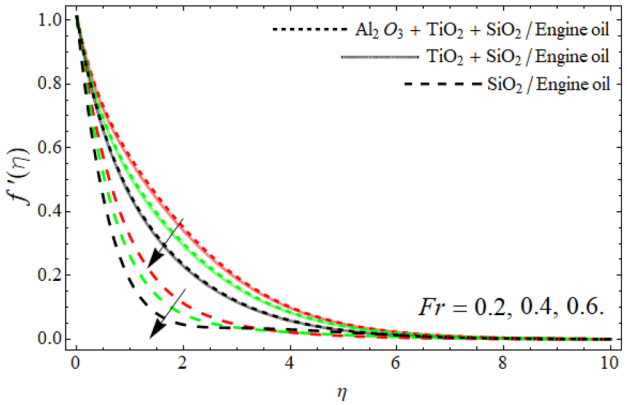

Figure 6. Velocity $f'(\eta)$ field versus *Fr*.

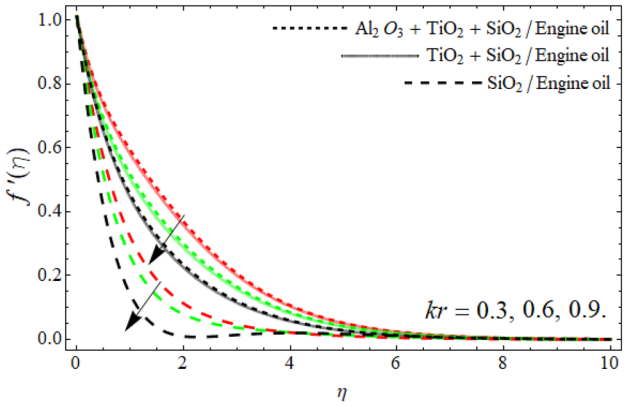

Figure 7. Velocity $f'(\eta)$ field versus porosity term *kr*.

The power-law component is designed to evaluate the fluid category's behavior between layers. It's worth noting that m is a non-dimensional quantity generated as a result of the Carreau Yasuda fluid. When *m* is raised, the velocity curve shrinkages. Frictional forces are formed between momentum layers, and frictional forces cause fluid to thicken as shown in Fig. 5. Figures 6 and 7 revealed that the velocity outlines diminish with the upshot of Darcy Forchheimer's term *Fr* and porosity term. The rising effect of Darcy and porosity term enhances with the porosity of the vertical stretching surface, which resists the fluid flow, as result, the velocity field drops.

Figures 8, 9, 10, 11 exposed the nature of energy $\theta(\eta)$ curve versus the variation of ferrohydrodynamic interaction number β, heat source term H_t, Eckert number *Ec* and ternary nanoparticles φ respectively. It can

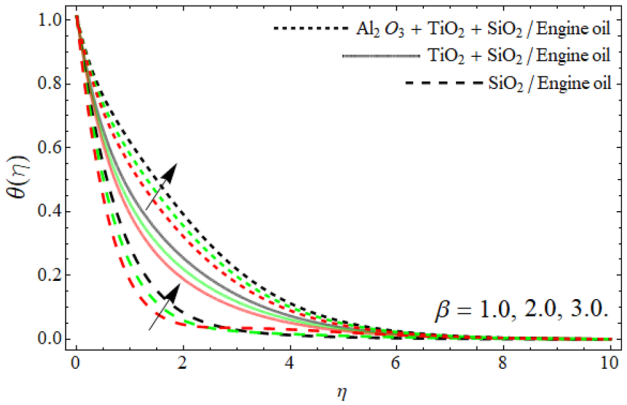

Figure 8. The energy $\theta(\eta)$ outlines versus ferrohydrodynamic interaction number β.

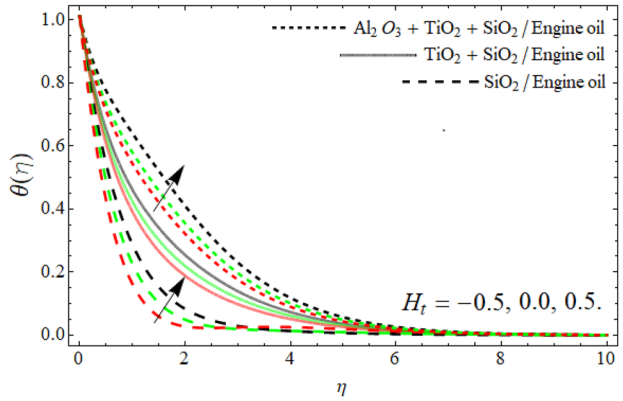

Figure 9. The energy $\theta(\eta)$ outlines versus H_t.

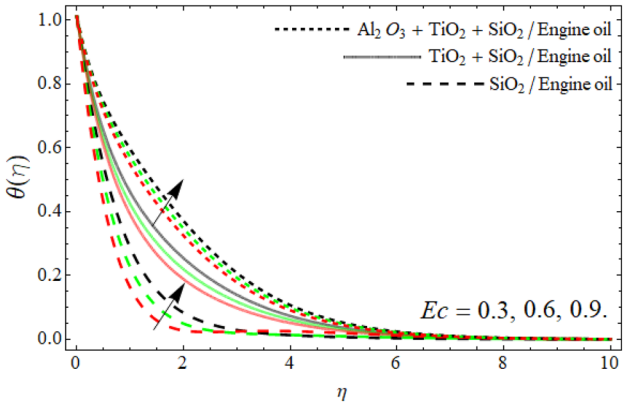

Figure 10. The energy $\theta(\eta)$ outlines versus Eckert number Ec.

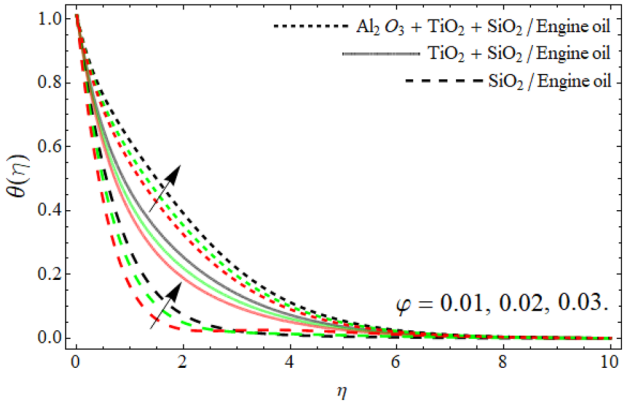

Figure 11. The energy profile $\theta(\eta)$ outlines versus ternary nanoparticles φ.

be perceived that the upshot of all parameters β, H_t, Ec and φ significantly boosts the energy profile. The magnetic dipole draws fluid molecules at the wall's surface, and this pulling of fluid droplets toward the magnetic dipole causes friction between layers and particles. Hence, the energy profile of ternary nanofluid enhances as depicted in Fig. 8. The influence of heat source term and Eckert number results in the additional heat inside the fluid flow, which causes the inclination of the temperature field as shown in Figs. 9 and 10. Figure 11 reported that the inclusion of nano particulates in the base fluid amplifies the energy profile. The density of engine oil as compared to Al_2O_3, SiO_2 and TiO_2 is much higher. Therefore, the insertion of these nanoparticles into the engine oil reduces its average density. On the other hand, the thermal conductivity of trihybrid nanoparticles is greater

than base fluid, that's why, the dispersion of the nano particulates, enhances the thermal profile of trihybrid nanofluids as shown in Fig. 11.

Tables 1 and 2 demonstrate the experimental values of ternary hybrid nanoparticles and engine oil and the basic mathematical model used for the simulation of trihybrid nanofluid flow. The consequences of skin friction and Nusselt number on Weissenberg number, viscous dissipation, heat source and power-law term are plotted in Table 3. Table 3 shows that greater numeric quantities of the heat source factor result in declination in heat transfer and flow rate. When the Weissenberg number is elevated, however, the flow rate improves. The importance of the power-law number in developing the highest quantity of heat transference rate and the flow rate has been noted.

	k	σ	ρ
Engine oil	0.144	0.125×10^{-11}	884
Al_2O_3	32.9	5.96×10^{7}	6.310
TiO_2	8.953	2.4×10^{6}	4.250
SiO_2	1.4013	3.5×10^{6}	2.270

Table 1. The investigational values of Al_2O_3, SiO_2, TiO_2 and engine oil[40].

Viscosity	$\frac{\mu_{Thnf}}{\mu_f} = \frac{1}{(1-\phi_{Al_2O_3})^{2.5}(1-\phi_{TiO_2})^{2.5}(1-\phi_{SiO_2})^{2.5}}$,
Density	$\frac{\rho_{Thnf}}{\rho_f} = (1-\phi_{TiO_2})\left[(1-\phi_{TiO_2})\left\{(1-\phi_{SiO_2})+\phi_{SiO_2}\frac{\rho_{SiO_2}}{\rho_f}\right\}+\phi_{TiO_2}\frac{\rho_{TiO_2}}{\rho_f}\right]+\phi_{Al_2O_3}\frac{\rho_{Al_2O_3}}{\rho_f}$,
Specific heat	$\frac{(\rho cp)_{Thnf}}{(\rho cp)_f} = \phi_{Al_2O_3}\frac{(\rho cp)_{Al_2O_3}}{(\rho cp)_f}+(1-\phi_{Al_2O_3})\left[(1-\phi_{TiO_2})\left\{(1-\phi_{SiO_2})+\phi_{SiO_2}\frac{(\rho cp)_{SiO_2}}{(\rho cp)_f}\right\}+\phi_{TiO_2}\frac{(\rho cp)_{TiO_2}}{(\rho cp)_f}\right]\right\}$
Thermal conduction	$\frac{k_{Thnf}}{k_{hnf}} = \left(\frac{k_{SiO_2}+2k_{hnf}-2\phi_{SiO_2}(k_{hnf}-k_{SiO_2})}{k_{SiO_2}+2k_{hnf}+\phi_{SiO_2}(k_{hnf}-k_{SiO_2})}\right), \frac{k_{hnf}}{k_{nf}} = \left(\frac{k_{TiO_2}+2k_{nf}-2\phi_{TiO_2}(k_{nf}-k_{TiO_2})}{k_{TiO_2}+2k_{nf}+\phi_{TiO_2}(k_{nf}-k_{TiO_2})}\right),$ $\frac{k_{nf}}{k_f} = \left(\frac{k_{Al_2O_3}+2k_f-2\phi_{Al_2O_3}(k_f-k_{Al_2O_3})}{k_{Al_2O_3}+2k_f+\phi_{Al_2O_3}(k_f-k_{Al_2O_3})}\right),$
Electrical conductivity	$\frac{\sigma_{Thnf}}{\sigma_{hnf}} = \left(1+\frac{3\left(\frac{\sigma_{SiO_2}}{\sigma_{hnf}}-1\right)\phi_{SiO_2}}{\left(\frac{\sigma_{SiO_2}}{\sigma_{hnf}}+2\right)-\left(\frac{\sigma_{SiO_2}}{\sigma_{hnf}}-1\right)\phi_{SiO_2}}\right), \frac{\sigma_{hnf}}{\sigma_{nf}} = \left(1+\frac{3\left(\frac{\sigma_{TiO_2}}{\sigma_{nf}}-1\right)\phi_{TiO_2}}{\left(\frac{\sigma_{TiO_2}}{\sigma_{nf}}+2\right)-\left(\frac{\sigma_{TiO_2}}{\sigma_{nf}}-1\right)\phi_{TiO_2}}\right),$ $\frac{\sigma_{nf}}{\sigma_f} = \left(1+\frac{3\left(\frac{\sigma_{Al_2O_3}}{\sigma_f}-1\right)\phi_{Al_2O_3}}{\left(\frac{\sigma_{Al_2O_3}}{\sigma_f}+2\right)-\left(\frac{\sigma_{Al_2O_3}}{\sigma_f}-1\right)\phi_{Al_2O_3}}\right).$

Table 2. The thermal properties of trihybrid nanoliquids[40].

Parameters	Values	$-(Re)^{\frac{1}{2}}C_f$[44]	$-(\mathrm{Re})^{\frac{1}{2}}C_f$	$-(Re)^{-\frac{1}{2}}Nu$[44]	$-(Re)^{-\frac{1}{2}}Nu$
	0.0	0.2620880941	0.2620880862	0.6269013682	0.6269013784
We	0.5	0.2805115031	0.2805115133	0.6150054882	0.6150054981
	1.5	0.2983830010	0.2983830212	0.6038359770	0.6038359872
	− 1.5	0.4793858421	0.47938585213	0.3524512521	0.3524512623
H_t	0.0	0.3864732265	0.3864732366	0.2572567431	0.2572567533
	0.7	0.1464269369	0.1464269465	0.2116717874	0.2116717775
	0.1	0.0746743038	0.0746743237	0.3641187594	0.3641187793
m	0.4	0.1547000729	0.1547000828	0.5585378446	0.5585378647
	0.7	0.2398563119	0.2398563218	0.7083750632	0.7083750835
	0.0	0.2619120138	0.2619120339	0.7417200656	0.7417200755
λ	0.4	0.2614988160	0.2614988261	0.6310408286	0.6310408484
	0.8	0.2612510196	0.2612510397	0.5406325980	0.5406326871

Table 3. The statistical outputs of skin friction $-(Re)^{\frac{1}{2}}C_f$ and Nusselt number $-(Re)^{-\frac{1}{2}}Nu$ as well as its comparison with the existing literature.

Conclusion

We have studied the significances of magnetic dipole and heat transmission through ternary hybrid Carreau Yasuda nanoliquid flow across a vertical stretching sheet. The ternary compositions of Al_2O_3, SiO_2, and TiO_2-nps in the Carreau Yasuda fluid are used to prepare the Thnf. The heat transfer and velocity are observed in context of heat source/sink and Darcy Forchhemier effect. Mathematically, the flow scenario has been expressed in form of the nonlinear system of PDEs for fluid velocity and energy propagation. The obtained set of PDEs are transform into ODEs through suitable substitutions. The obtained dimensionless equations are computationally solved with the help of the PCM. The main outcomes are:

- The accumulation of Al_2O_3, SiO_2 and TiO_2-nps to the engine oil, advances the energy and momentum profiles.
- Relative to simple fluid, ternary hybrid nanofluid have a greater tendency to boost the energy transmission across a vertical plate.
- The fluid velocity $f'(\eta)$ lowers with the outcome of the ferrohydrodynamic interaction term, while enhances with the inclusion of nano particulates (Al_2O_3, SiO_2 and TiO_2) in the base fluid.
- The fluid velocity contour declines with the upshot of *We* and power-law number *m*.
- The escalating influence of Darcy Forchheimer's term and porosity constant reduces the velocity outlines.
- The energy contour $\theta(\eta)$ enhances with the variation of ferrohydrodynamic interaction number, heat source term, Eckert number and ternary nanoparticles.
- The rising effects of the power-law index remarkably elevate the skin friction and Nusselt number of trihybrids nanofluid.

Data availability

All data used in this manuscript have been presented within the article.

Received: 9 January 2023; Accepted: 21 March 2023
Published online: 03 April 2023

References

1. Algehyne, E. A., Alhusayni, Y. Y., Tassaddiq, A., Saeed, A., & Bilal, M. The study of nanofluid flow with motile microorganism and thermal slip condition across a vertical permeable surface. *Waves Random Complex Media*, 1–18 (2022).
2. Shah, N. A., Yook, S. J. & Tosin, O. Analytic simulation of thermophoretic second grade fluid flow past a vertical surface with variable fluid characteristics and convective heating. *Sci. Rep.* **12**(1), 1–17 (2022).
3. Chen, S., Zhao, W. & Wan, D. Turbulent structures and characteristics of flows past a vertical surface-piercing finite circular cylinder. *Phys. Fluids* **34**(1), 015115 (2022).
4. Singh, J. K. & Seth, G. S. Scrutiny of convective MHD second-grade fluid flow within two alternatively conducting vertical surfaces with Hall current and induced magnetic field. *Heat Transf.* **51**(8), 7613–7634 (2022).
5. Shafiq, A., Çolak, A. B. & Sindhu, T. N. Significance of bioconvective flow of MHD thixotropic nanofluid passing through a vertical surface by machine learning algorithm. *Chin. J. Phys.* **80**, 427–444 (2022).
6. Fayz-Al-Asad, M., Oreyeni, T., Yavuz, M. & Olanrewaju, P. O. Analytic simulation of MHD boundary layer flow of a chemically reacting upper-convected Maxwell fluid past a vertical surface subjected to double stratifications with variable properties. *Eur. Phys. J. Plus* **137**(7), 1–11 (2022).
7. Sharma, B. K. & Gandhi, R. Combined effects of Joule heating and non-uniform heat source/sink on unsteady MHD mixed convective flow over a vertical stretching surface embedded in a Darcy-Forchheimer porous medium. *Propuls. Power Res.* **11**(2), 276–292 (2022).
8. Sharma, B. K., Kumar, A., Gandhi, R. & Bhatti, M. M. Exponential space and thermal-dependent heat source effects on electro-magneto-hydrodynamic Jeffrey fluid flow over a vertical stretching surface. *Int. J. Mod. Phys. B* **36**(30), 2250220 (2022).
9. Rizk, D. *et al.* Impact of the KKL correlation model on the activation of thermal energy for the hybrid nanofluid (GO+ ZnO+ Water) flow through permeable vertically rotating surface. *Energies* **15**(8), 2872 (2022).
10. Rooman, M. *et al.* Electromagnetic trihybrid Ellis nanofluid flow influenced with a magnetic dipole and chemical reaction across a vertical surface. *ACS Omega* **7**(41), 36611–36622 (2022).
11. Prabhavathi, B., Reddy, P. S., Vijaya, R. B. & Chamkha, A. MHD boundary layer heat and mass transfer flow over a vertical cone embedded in porous media filled with Al_2O_3-water and Cu-water nanofluid. *J. Nanofluids* **6**(5), 883–891 (2017).
12. Sreedevi, P. & Sudarsana Reddy, P. Heat and mass transfer analysis of MWCNT-kerosene nanofluid flow over a wedge with thermal radiation. *Heat Transf.* **50**(1), 10–33 (2021).
13. Reddy, P. S., & Chamkha, A. J. Heat and mass transfer characteristics of al 2 o 3– water and ag– water nanofluid through porous media over a vertical cone with heat generation/absorption. *J. Porous Media* **20**(1). (2017).
14. Dadheech, A., Parmar, A., Agrawal, K., Al-Mdallal, Q. & Sharma, S. Second law analysis for MHD slip flow for Williamson fluid over a vertical plate with Cattaneo-Christov heat flux. *Case Stud. Therm. Eng.* **33**, 101931 (2022).
15. Ghoranneviss, M., Soni, A., Talebitaher, A., & Aslan, N. Nanomaterial synthesis, characterization, and application. *J. Nanomater* **2015** (2015).
16. Haq, I., Bilal, M., Ahammad, N. A., Ghoneim, M. E., Ali, A., & Weera, W. Mixed convection nanofluid flow with heat source and chemical reaction over an inclined irregular surface. *ACS Omega* (2022)
17. Elattar, S. *et al.* Computational assessment of hybrid nanofluid flow with the influence of hall current and chemical reaction over a slender stretching surface. *Alex. Eng. J.* **61**(12), 10319–10331 (2022).
18. Saidur, R., Leong, K. Y. & Mohammed, H. A. A review on applications and challenges of nanofluids. *Renew. Sustain. Energy Rev.* **15**(3), 1646–1668 (2011).
19. Alharbi, K. A. M. *et al.* Computational valuation of Darcy ternary-hybrid nanofluid flow across an extending cylinder with induction effects. *Micromachines* **13**(4), 588 (2022).
20. Sudarsana Reddy, P., Jyothi, K. & Suryanarayana Reddy, M. Flow and heat transfer analysis of carbon nanotubes-based Maxwell nanofluid flow driven by rotating stretchable disks with thermal radiation. *J. Braz. Soc. Mech. Sci. Eng.* **40**(12), 576 (2018).
21. Okumura, M. *et al.* Chemical vapor deposition of gold on Al_2O_3, SiO_2, and TiO_2 for the oxidation of CO and of H_2. *Catal. Lett.* **51**(1), 53–58 (1998).
22. Minea, A. A. Hybrid nanofluids based on Al_2O_3, TiO_2 and SiO_2: Numerical evaluation of different approaches. *Int. J. Heat Mass Transf.* **104**, 852–860 (2017).

23. Said, Z., Kamyar, A. & Saidur, R. Experimental investigation on the stability and density of TiO_2, Al_2O_3, SiO_2 and $TiSiO_4$. *IOP Conf. Series Earth Environ. Sci.* **16**(1), 012002 (2013).
24. Minea, A. A. Pumping power and heat transfer efficiency evaluation on Al_2O_3, TiO_2 and SiO_2 single and hybrid water-based nanofluids for energy application. *J. Therm. Anal. Calorim.* **139**(2), 1171–1181 (2020).
25. Abbasi, A. *et al.* A comparative thermal investigation for modified hybrid nanofluid model (Al_2O_3–SiO_2–TiO_2)/($C_2H_6O_2$) due to curved radiated surface. *Case Stud. Therm. Eng.* **37**, 102295 (2022).
26. Dadheech, P. K., Agrawal, P., Sharma, A., Nisar, K. S. & Purohit, S. D. Transportation of Al_2O_3-SiO_2-TiO_2 modified nanofluid over an exponentially stretching surface with inclined magnetohydrodynamic. *Therm. Sci.* **25**, 279–285 (2021).
27. Erkan, A., Tüccar, G., Tosun, E. & Özgür, T. Comparison of effects of nanofluid utilization (Al_2O_3, SiO_2, TiO_2) with reference water in automotive radiators on exergetic properties of diesel engines. *SN Appl. Sci.* **3**(3), 1–13 (2021).
28. Alharbi, K. A. M., Bani-Fwaz, M. Z., Eldin, S. M. & Yassen, M. F. Numerical heat performance of TiO_2/Glycerin under nanoparticles aggregation and nonlinear radiative heat flux in dilating/squeezing channel. *Case Stud. Therm. Eng.* **41**, 102568 (2023).
29. Alharbi, K. A. M., Ashraf, W., Eldin, S. M., Yassen, M. F. & Jamshed, W. Applied heat transfer modeling in conventional hybrid (Al_2O_3-CuO)/$C_2H_6O_2$ and modified-hybrid nanofluids (Al_2O_3-CuO-Fe_3O_4)/$C_2H_6O_2$ between slippery channel by using least square method (LSM). *AIMS Math.* **8**(2), 4321–4341 (2023).
30. Alharbi, M., Abdulkhaliq, K. & Adnan, A. Thermal investigation and physiochemical interaction of H_2O and $C_2H_6O_2$ saturated by Al_2O_3 and γAl_2O_3 nanomaterials. *J. Appl. Biomater. Funct. Mater.* **20**, 22808000221136484 (2022).
31. Reddy, P. S., Sreedevi, P., Chamkha, A. J., & Al-Mudhaf, A. F. Heat and mass transfer boundary-layer flow over a vertical cone through porous media filled with a Cu–water and Ag–water nanofluid. *Heat Transf. Res.* **49**(2) (2018).
32. Sreedevi, P., Reddy, P. S. & Sheremet, M. A comparative study of Al2O3 and TiO2 nanofluid flow over a wedge with non-linear thermal radiation. *Int. J. Numer. Meth. Heat Fluid Flow* **30**(3), 1291–1317 (2020).
33. Sreedevi, P. & Reddy, P. S. Entropy generation and heat transfer analysis of alumina and carbon nanotubesbased hybrid nanofluid inside a cavity. *Phys. Scr.* **96**(8), 085210 (2021).
34. Bilal, M., Ullah, I., Alam, M. M., Weera, W. & Galal, A. M. Numerical simulations through PCM for the dynamics of thermal enhancement in ternary MHD hybrid nanofluid flow over plane sheet, cone, and wedge. *Symmetry* **14**(11), 2419 (2022).
35. Gul, T. *et al.* Magnetic dipole impact on the hybrid nanofluid flow over an extending surface. *Sci. Rep.* **10**(1), 1–13 (2020).
36. Bashir, S. *et al.* Magnetic dipole and thermophoretic particle deposition impact on bioconvective oldroyd-B fluid flow over a stretching surface with Cattaneo-Christov heat flux. *Nanomaterials* **12**(13), 2181 (2022).
37. Shoaib, M. *et al.* Soft computing paradigm for Ferrofluid by exponentially stretched surface in the presence of magnetic dipole and heat transfer. *Alex. Eng. J.* **61**(2), 1607–1623 (2022).
38. Nadeem, S., Ahmad, S. & Muhammad, N. Analysis of ferrite nanoparticles in liquid. *Pramana* **94**(1), 1–9 (2020).
39. Muhammad, N. & Nadeem, S. Ferrite nanoparticles Ni-$ZnFe_2O_4$, Mn-$ZnFe_2O_4$ and Fe_2O4 in the flow of ferromagnetic nanofluid. *Eur. Phys. J. Plus* **132**(9), 1–12 (2017).
40. Hou, E. *et al.* Dynamics of tri-hybrid nanoparticles in the rheology of pseudo-plastic liquid with dufour and soret effects. *Micromachines* **13**(2), 201 (2022).
41. Shuaib, M., Shah, R. A., Durrani, I. & Bilal, M. Electrokinetic viscous rotating disk flow of Poisson-Nernst-Planck equation for ion transport. *J. Mol. Liq.* **313**, 113412 (2020).
42. Shuaib, M., Shah, R. A. & Bilal, M. Variable thickness flow over a rotating disk under the influence of variable magnetic field: An application to parametric continuation method. *Adv. Mech. Eng.* **12**(6), 1687814020936385 (2020).
43. Alrabaiah, H., Bilal, M., Khan, M. A., Muhammad, T. & Legas, E. Y. Parametric estimation of gyrotactic microorganism hybrid nanofluid flow between the conical gap of spinning disk-cone apparatus. *Sci. Rep.* **12**(1), 1–14 (2022).
44. Wang, F. *et al.* An implication of magnetic dipole in Carreau Yasuda liquid influenced by engine oil using ternary hybrid nanomaterial. *Nanotechnol. Rev.* **11**(1), 1620–1632 (2022).

Acknowledgements

The authors are thankful to the Deanship of Scientific Research, King Khalid University, Abha, Saudi Arabia, for financially supporting this work through the General Research Project under Grant No. R.G.P.1/125/43.

Author contributions

M.B. and I.U. wrote the manuscript and presented the numerical simulations. M.M.A. thoroughly reviewed the mathematical calculation and restructured the manuscript. S.I.S. and S.M.E. revised the manuscript and verified the governing equations and validate the numerical results. They also helped in the funding acquisition. All authors are agreed on the final draft of the submission file.

Competing interests

The authors declare no competing interests.

Additional information

Correspondence and requests for materials should be addressed to S.M.E.

Reprints and permissions information is available at www.nature.com/reprints.

Publisher's note Springer Nature remains neutral with regard to jurisdictional claims in published maps and institutional affiliations.